



Synthesis of Programmable Reaction-Diffusion Fronts Using DNA Catalyzers

Anton Zadorin, Yannick Rondelez, Jean-Christophe Galas, André
Estévez-Torres

► **To cite this version:**

Anton Zadorin, Yannick Rondelez, Jean-Christophe Galas, André Estévez-Torres. Synthesis of Programmable Reaction-Diffusion Fronts Using DNA Catalyzers. *Physical Review Letters*, American Physical Society, 2015, 114 (6), pp.55 - 66. <10.1103/PhysRevLett.114.068301>. <hal-01623547>

HAL Id: hal-01623547

<http://hal.upmc.fr/hal-01623547>

Submitted on 25 Oct 2017

HAL is a multi-disciplinary open access archive for the deposit and dissemination of scientific research documents, whether they are published or not. The documents may come from teaching and research institutions in France or abroad, or from public or private research centers.

L'archive ouverte pluridisciplinaire **HAL**, est destinée au dépôt et à la diffusion de documents scientifiques de niveau recherche, publiés ou non, émanant des établissements d'enseignement et de recherche français ou étrangers, des laboratoires publics ou privés.

Synthesis of programmable reaction-diffusion fronts using DNA catalyzers

Anton S. Zadorin,¹ Yannick Rondelez,² Jean-Christophe Galas,¹ and André Estevez-Torres^{1,*}

¹*Laboratoire de photonique et de nanostructures,
CNRS, route de Nozay, 91460 Marcoussis, France*

²*LIMMS/CNRS-IIS, University of Tokyo, Komaba 4-6-2 Meguro-ku, Tokyo, Japan*

(Dated: March 6, 2015)

We introduce a DNA-based reaction-diffusion (RD) system in which reaction and diffusion terms can be precisely and independently controlled. The effective diffusion coefficient of an individual reaction component, as we demonstrate on a traveling wave, can be reduced up to 2.7-fold using a self-assembled hydrodynamic drag. The intrinsic programmability of this RD system allows us to engineer, for the first time, orthogonal autocatalysts that counter-propagate with minimal interaction. Our results are in excellent quantitative agreement with predictions of the Fisher-Kolmogorov-Petrovskii-Piscunov model. These advances open the way for the rational engineering of pattern formation in pure chemical RD systems.

Reaction-diffusion (RD) models are a rich source of spatiotemporal pattern formation phenomena. Not only is this mechanism relevant to biological morphogenesis [1], but it is one of the few conceptualizations that physics can offer for the spontaneous emergence of order in molecular systems [2]. Traveling waves [3], spirals [4] and Turing patterns [5], among other structures [6, 7], have been observed experimentally. However, in contrast to pattern formation in hydrodynamics, few of these studies are quantitative [8, 9]. The reason is that we lack a fully controllable and easily modeled experimental RD system. In addition, to generate arbitrary spatiotemporal patterns the following properties need to be programmable: i) the topology of the chemical reaction network (CRN), ii) the reaction rates, and iii) the diffusion coefficients of individual species D_i . The majority of attempts to achieve these goals concern redox or acid-base reactions related to the Belousov-Zhabotinsky (BZ) reaction [10–12]. Our current understanding does not allow to engineer CRNs with such chemistries in a rational way. Although semi-heuristic methods have been developed [13–15], they are neither general nor modular. Particular solutions to control diffusion have been devised for BZ-related reactions [5, 16] but no general strategy is available.

DNA-based chemical reaction networks provide an interesting solution to the issues mentioned above. Due to base complementarity, the kinetics of the DNA hybridization reaction can be predicted from the sequence [17, 18]. Recent advances in DNA nanotechnology allow us to program the topology of quite complex CRNs. Enzyme-free DNA circuits have been used for producing tunable cascading reactions [19] and encoding edge detection algorithms [20]. In combination with enzymatic reactions, non-equilibrium dissipative behaviors with DNA circuits have been obtained, such as non-linear oscillators [21–23], memory switches [24], and propagating waves and spirals [25].

Here we introduce a general method to control specifically the reaction and diffusion rates of DNA species

involved in such programmable reaction networks. We demonstrate this on the minimal reaction capable of self-organization in space: an autocatalytic front propagating in a 1-dimensional reactor. As such, we used an autocatalytic node of the DNA polymerase exonuclease nicking enzyme (PEN) toolbox, that works as follows [21]. Species A, an 11-mer single-stranded DNA (ssDNA), catalyzes its own growth in the presence of a template strand T, a 22-mer that carries two contiguous domains complementary to A: species A reversibly hybridizes with T on either of these domains and one of the resulting complexes can be extended by a polymerase (pol), which is the rate-limiting step in our conditions. The resulting double-stranded DNA (dsDNA) complex carries a recognition site for a nicking enzyme (nick) such that the upper strand is cut at its midpoint, releasing two molecules of A and the intact T. The kinetics of this process is captured by the simplified mechanism sketched in (FIG. 1a, for details refer to [21, 25]). The total concentration of each species, free or bound, is noted in italics in the following.

In a one dimensional reactor the evolution of A is described by the reaction-diffusion equation

$$\frac{\partial A}{\partial t} = r(A) + \frac{\partial}{\partial x} \left(D_{\text{eff}}(A) \frac{\partial A}{\partial x} \right), \quad (1)$$

where $r(A)$ is the reaction term, and we have made explicit that the effective diffusion coefficient $D_{\text{eff}}(A)$ depends on A . This reflects the existence of A in states with different diffusion coefficients (free and bound to T). When $D_{\text{eff}}(A) = D$, equation (1) together with reasonable assumptions about $r(A)$ [26], form the Fisher-Kolmogorov-Petrovskii-Piscunov (Fisher-KPP) case: there exists a single stable asymptotic traveling wave solution $A(x, t) = A(x - v_m t)$, where $v_m = 2\sqrt{r'(0)D}$ depends neither on other details of the growth function $r(A)$ nor on the shape of the initial condition [27, 28]. In our case, if the front propagation is controlled by the growth at the leading edge, where $A \simeq 0$,

we can assume [29]

$$D = D_{\text{eff}}(0) \approx \frac{K}{2T_0 + K} D_A + \frac{2T_0}{2T_0 + K} D_{A:T}, \quad (2)$$

where K is the dissociation constant of A with its complementary sequence in T, T_0 the total concentration of T and D_A and D_T are the diffusion coefficients of free A and free T, respectively. In the following we approximate $D_{A:T}$ by D_T . We thus have,

$$v_m = 2\sqrt{r'(0)D_{\text{eff}}(0)}. \quad (3)$$

To take into account deviations between our experiments and the model described above we introduce a phenomenological correction factor γ such that $v = \gamma v_m$, where v is the experimentally measured velocity and v_m is given by (2, 3). We hypothesize that γ results from considering the complex growth of A (involving several DNA hybridization and enzymatic reactions) as a single step $A \rightarrow 2A$ with a single average species A. We will demonstrate that our programmable molecular system is in quantitative agreement with the model when $\gamma = 1.3$.

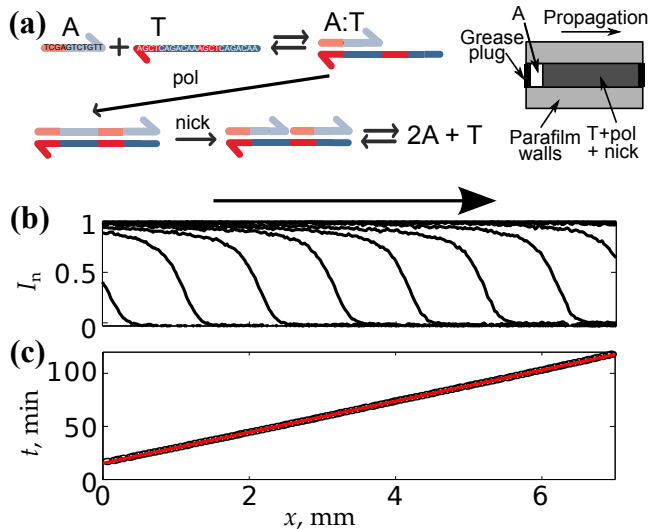


FIG. 1. A DNA-based autocatalyst generates a front traveling with uniform velocity in a channel reactor. (a) Simplified mechanism of the autocatalytic growth of A on T (left) and sketch of the experimental setup (right). (b) Experimental profiles of normalized fluorescence intensity I_n along the channel length, x , in 15 min intervals. The arrow shows the direction of propagation. (c) Time vs. the position of the front (linear fit in red). $T_0 = 200$ nM, 38°C .

In our experiments, A was indirectly monitored using the non-specific fluorescent DNA binder EvaGreen. An elongated channel ($2\text{ cm} \times 2\text{ mm} \times 200\text{ }\mu\text{m}$) was fabricated by thermally bonding a precut Parafilm sheet between two polystyrene slides (FIG. 1a). The channel was first filled with a solution containing all components

(T, enzymes and deoxyribonucleotides) except A. Subsequently, $1\text{ }\mu\text{M}$ of A was injected to the left inlet using a micropipette [30]. After sealing the two ends to prevent evaporation and hydrodynamic flow, the fluorescence intensity in the channel was recorded using a microscope equipped with a $2.5\times$ objective and a CCD camera. We observed a front of fluorescence that moved from left to right (FIG. 1bc). The shape of the intensity profile along x was stable in time. The front propagated at a constant velocity of $65 \pm 5\text{ }\mu\text{m}/\text{min}$ for about 150 min before reaching the right end of the channel. The observed velocity did not depend on the injection step nor on the injected concentration of A, in agreement with the Fisher-KPP case. In a set of independent experiments we measured $r'(0)$, D_A , D_T and K . We measured $r'(0) = 0.077 \pm 0.013\text{ min}^{-1}$ by recording the fluorescence intensity as a function of time, which was exponential at short times (and low A), in a well-mixed reactor [31]. We measured $D_A = (16 \pm 3) \times 10^3\text{ }\mu\text{m}^2/\text{min}$ and $D_T = (10.7 \pm 0.7) \times 10^3\text{ }\mu\text{m}^2/\text{min}$ at 38°C from the relaxation of a sharp initial concentration profile. As an approximation for K we measured the dissociation constant of the hybridization of A with its complementary strand and found $K = 3\text{ nM}$ at 38°C . From (2,3) our model predicts $v_m = 59 \pm 7\text{ }\mu\text{m}/\text{min}$, which is just 10% below the experimental value ($\gamma = v/v_m = 1.1 \pm 0.2$).

To check the scaling $v \sim (r'(0))^{1/2}$, and the capability of the model to provide a quantitative prediction of v with a unique value of γ , we measured $r'(0)$ and v for different T_0 and pol (FIG. 2, [32]). FIG. 2a,b shows the dependence on T_0 . The growth of the autocatalyst was always exponential at short times, with a linear dependence, $r'(0) = (3.1 \times 10^{-4}\text{ nM}^{-1}\text{ min}^{-1}) \times T_0$, in the range $T_0 = 0\text{--}100\text{ nM}$. The growth rate can thus be specifically tuned by changing T_0 —an important feature for modular programmability (FIG. 2a). The velocity of the front also depended on T_0 . Fronts propagated faster as T_0 increased. Since we found $r'(0) \sim T_0$, (3) predicted $v^2 \sim T_0$, which was verified experimentally for $T_0 = 0\text{--}200\text{ nM}$. We used the values of D_i , K and $r'(0)$ reported above to calculate v_m with (2,3) resulting in $\gamma = 1.30 \pm 0.16$, in agreement with the value reported above. With $\gamma = 1.3$, (3) is in excellent agreement with the data (FIG. 2b, blue line). Note that A in the back of the front increased with T_0 . The good agreement between the model and the experiment in FIG. 2b thus supports our approximation $D_{\text{eff}}(A) \approx D_{\text{eff}}(0)$.

Control experiments showed that the reaction rate was limited by the polymerization step rather than by the subsequent cleavage by the nickase. We thus expected $r'(0) \sim pol$ which gave us another opportunity to verify the validity of the scaling predicted by the Fisher-KPP model. As a test of the robustness of the model's predictions, we verified this scaling at a different temperature, 44°C , and nicking enzyme concentration, $500\text{ U}/\text{mL}$ (FIG. 2c,d). $r'(0)$ linearly depended on pol ,

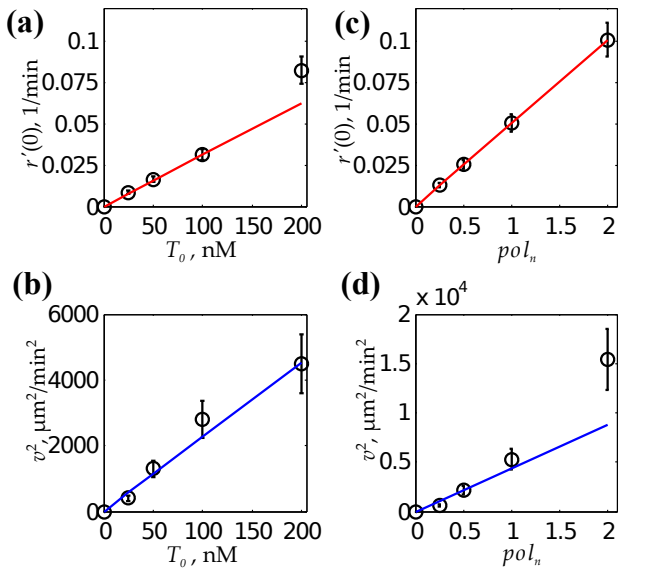


FIG. 2. The growth rate of the autocatalyst, $r'(0)$, (a), (c) and its propagation velocity, v , (b), (d) can be tuned specifically with the template concentration, T_0 , and non-specifically with the normalized polymerase concentration, pol_n . The red line is a linear fit for $T_0 = 0\text{--}100$ nM (a) and $pol_n = 0\text{--}2$. Blue lines are predictions using (2,3) with $\gamma = 1.3$. Experimental conditions: (a),(b) 38°C , (c),(d) 44°C . $pol_n = pol/(16 \text{ U/mL})$. Error bars for $r'(0)$ and v were estimated from 4 independent experiments at $T_0 = 200$ nM.

with $r'(0) = (0.05 \text{ min}^{-1}) \times pol_n$ in the range $pol_n = 0\text{--}2$. In the range $pol_n = 0\text{--}1$, $v^2 \sim pol_n$, and the velocities predicted by (2,3) with $\gamma = 1.3$ were, again, in excellent agreement with the experimental ones (FIG. 2d, blue line) [33]. Only for $pol_n = 2$ v was underestimated by the model. We speculate that this nonlinear effect may come from a transition from a pulled (Fisher-KPP, $r'(A) \leq r'(0)$) to a pushed front ($r'(A) > r'(0)$) [34].

In addition to controlling reaction rates, the ability to change diffusion coefficients is essential for pattern formation. For instance, no Turing bifurcation is possible with equal diffusion coefficients in a homogeneous system [10]. The validity of (3) provides an experimental way to measure changes in $D_{\text{eff}}(0)$ and thus monitor our capacity for controlling diffusion. Tuning the diffusion coefficient, D , of a molecule is not a simple task. Indeed, for a random coil, $D \sim M^{-1/2}$, where M is the molecular mass. As a result, to reduce D significantly relatively large molecular entities are needed. However, these entities need not necessarily be covalent or even stable: if A interacts dynamically with a ligand, its effective diffusion coefficient $D_{\text{eff}}(0)$ will be a weighted average between the free state with high D and the bound state with low D , as illustrated in (2). This approach applies well to single stranded DNA species, for which a binding partner always exist as its Watson-Crick complementary. The

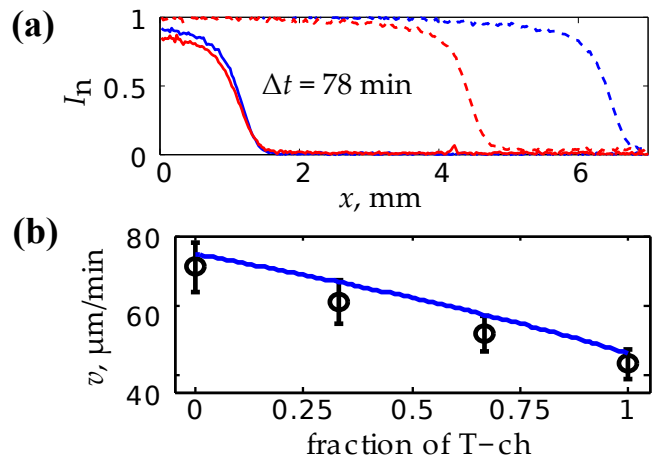


FIG. 3. The diffusion coefficient of the propagating species can be finely tuned using a hydrodynamic drag. (a) Fluorescence profiles of propagating fronts generated by T:trit (blue) and T-ch:trit (red) in different channels, at $t = 0$ min (solid lines) and $t = 78$ min (dashed). (b) Fine-tuning of the front velocity through diffusion by changing the molar fraction of T-ch compared to T and keeping $T_0 + T\text{-}ch_0 = 200$ nM constant, the line is the theoretical prediction from (2,3) with $\gamma = 1.3$. 10 g/L triton X-100, 38°C .

task then breaks down to reducing the diffusion of that partner.

The strategy chosen here consists of attaching a hydrodynamic drag to the 3'-end of template T, which binds to the active species A. We used a T modified with a hydrophobic cholesteryl group in 3' (that we note T-ch) in a 10 g/L triton X-100 solution. At this concentration this surfactant forms micelles about 5.5 nm in radius [35]. The cholesteryl group is expected to reversibly attach to them through hydrophobic interactions and form species T-ch:trit, with lower diffusion.

Figure 3a shows the propagation of a front of A growing on either T or T-ch in a triton solution with the same reaction conditions [36]. The second front advances 1.6 ± 0.2 times slower, the velocities being 65 ± 5 and $40 \pm 4 \text{ }\mu\text{m/min}$, respectively (confidence 0.95). In contrast, the influence of the triton drag on the growth kinetics appeared to be negligible. We measured $r'(0) = 0.078 \pm 0.005 \text{ min}^{-1}$ for T-ch:trit, which is identical, within experimental error, to the growth rate for T [37]. These values, according to (3), give $D_{\text{eff}}(0) = (5.1 \pm 1.1) \times 10^3 \text{ }\mu\text{m}^2/\text{min}$, corresponding to a (2.7 ± 0.8) -fold reduction in the diffusion coefficient of the propagating species. To compare them with the prediction given by (2), we independently measured the diffusion coefficient of T-ch:trit, and obtained $D_{\text{T-ch:trit}} = (4.0 \pm 0.3) \times 10^3 \text{ }\mu\text{m}^2/\text{min}$. Supposing that the hybridization constant is not affected by the presence of triton and taking thus $K = 3 \text{ nM}$, together with $\gamma = 1.3$, the predicted velocity for the front based on T-ch is $46 \pm 2 \text{ }\mu\text{m/min}$ and the theoretical expectation of the

change of $D_{\text{eff}}(0)$ in the presence of a drag is (2.6 ± 0.2) -fold. In addition, in a channel containing both T and T-ch:trit, we achieved fine tuning of the velocity of a front of A by varying the molar fraction of T-ch:trit while keeping the total concentration (T+T-ch:trit) constant (FIG. 3b). The theoretical prediction (2, 3) with the phenomenological correction $\gamma = 1.3$ was, in all these experiments, in excellent agreement with the experimental data without fitting, indicating that the diffusion coefficient of a propagating autocatalyst can be tuned in a quantitative manner.

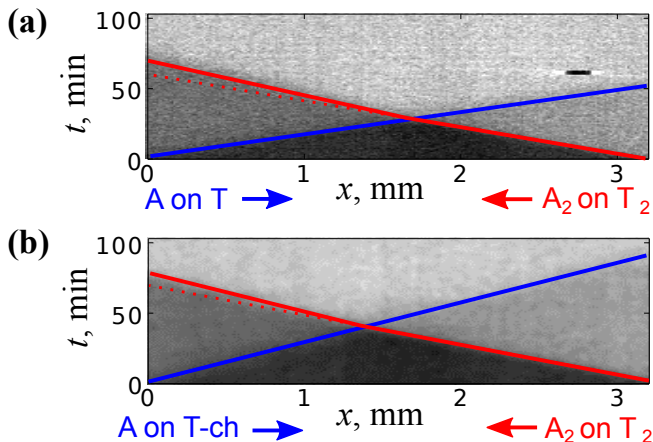


FIG. 4. Two independent autocatalysts counter-propagate with minimal interaction. Kymographs (time vs. position) for a front of A (blue), propagating from left to right, and a front of A_2 (red), propagating from right to left. (a) A grows on T. (b) A grows on T-ch:trit. Dark, semi-bright, and bright areas correspond to space with 0, 1, or 2 propagating fronts, respectively. Lines are visual guides to show the position of the front, with dashed indicating constant velocity of A_2 . $T_0 = T\text{-}ch_0 = T_{2,0} = 150$ nM, 10 g/l of triton X-100, 38°C.

Finally, to demonstrate the potential of our approach to run different non-interacting modules in the same reactor, we designed a second autocatalyst orthogonal to A: A_2 produced by template T_2 . A_2 had a different base at every sequence position of its template and depended on a different nicking enzyme. Its growth was slightly faster: $r'(0) = 0.13 \text{ min}^{-1}$ for $T_{2,0} = 200$ nM. In a channel containing a mix of T and T_2 two fronts propagating in opposite directions could be triggered by injecting A and A_2 on the left and right inlet, respectively (FIG. 4a and [38]). For $T_0 = T_{2,0} = 150$ nM; at $t < 32$ min each front propagated in a fresh medium and they behaved as independent fronts, as expected. When the two fronts encountered each other, A maintained its velocity constant and equal to $54 \mu\text{m}/\text{min}$ while the velocity of A_2 was reduced 1.3-fold from 48 to $37 \mu\text{m}/\text{min}$. The minimal interaction between the two fronts is particularly striking. It results from the fact that A and A_2 grow on

quasi-independent resources; the slight interaction coming from them sharing pol. This situation is very different from classic BZ systems where two colliding fronts annihilate because they need the same chemicals to grow. To the best of our knowledge this is the first time that the counter-propagation of two chemically distinct fronts is observed. In this configuration, substituting T by T-ch allowed us to specifically control the effective diffusion coefficient of A, given by (2), without perturbing that of A_2 (FIG. 4b). The velocity of A growing on T-ch:trit was $32 \mu\text{m}/\text{min}$ before and after the encounter, which corresponds, again, to a velocity reduction factor of 1.7 due to the drag. The velocities of A_2 before and after the encounter were the same as reported above.

The modularity of the PEN DNA toolbox hence allows to simply design *de novo* autocatalysts which spatiotemporal behavior can be quantitatively predicted. Beyond its striking programmability, the system presented here is commercially available and it does not require particular skills in biochemistry. For these reasons, we believe that it will be widely used to investigate fascinating questions about the emergence of spatiotemporal molecular order [39].

This research was supported by ANR jeunes chercheurs under award Dynano. A.S.Z. acknowledges a postdoctoral fellowship from NanoSciences Ile-de-France (Enginets award) and from the Laboratoire d'Excellence en Nanoscience et Nanotechnologie Nanosacly (Turnano award). We thank A. Kalley and M. Cabon for preliminary experiments. We are indebted to L. Jullien, C. Gosse and T. Le Saux (ENS, Paris) with whom the idea of diffusion control arose and to D. Baigl (ENS, Paris) for fruitful discussions.

* aestevez@lpn.cnrs.fr

- [1] S. Kondo and T. Miura, *Science* **329**, 1616 (2010), doi: 10.1126/science.1179047.
- [2] M. C. Cross and P. C. Hohenberg, *Rev. Mod. Phys.* **65**, 851 (1993).
- [3] A. N. Zaikin and A. M. Zhabotinsky, *Nature* **225**, 535 (1970), doi: 10.1038/225535b0.
- [4] A. T. Winfree, *Science* **175**, 634 (1972).
- [5] V. Castets, E. Dulos, J. Boissonade, and P. De Kepper, *Phys. Rev. Lett* **64**, 2953 (1990).
- [6] K.-J. Lee, W. D. McCormick, J. E. Pearson, and H. L. Swinney, *Nature* **369**, 215 (1994), doi: 10.1038/369215a0.
- [7] V. K. Vanag and I. R. Epstein, *Int. J. Dev. Biol.* **53**, 673 (2009).
- [8] R. J. Field and R. M. Noyes, *J. Am. Chem. Soc.* **96**, 2001 (1974), doi: 10.1021/ja00814a003.
- [9] A. Hanna, A. Saul, and K. Showalter, *J. Am. Chem. Soc.* **104**, 3838 (1982), doi: 10.1021/ja00378a011.
- [10] I. Epstein and J. A. Pojman, *An introduction to nonlinear chemical reactions* (Oxford University Press, New York, 1998).
- [11] F. Sagues and I. R. Epstein, *J. Chem. Soc., Dalton Trans*

- , 1201 (2003).
- [12] V. K. Vanag and I. R. Epstein, *Chaos* **18**, 026107 (2008).
- [13] J. Boissonade and P. De Kepper, *J. Phys. Chem* **84**, 501 (1980), doi: 10.1021/j100442a009.
- [14] P. De Kepper, I. R. Epstein, K. Kustin, and M. Orban, *J. Phys. Chem* **86**, 170 (1982).
- [15] J. Horvath, I. Szalai, and P. De Kepper, *Science* **324**, 772 (2009), doi: 10.1126/science.1169973.
- [16] V. K. Vanag and I. R. Epstein, *Science* **294**, 835 (2001).
- [17] M. Zuker, *Nucleic acids res.* **31**, 3406 (2003), 10.1093/nar/gkg595.
- [18] D. Y. Zhang and E. Winfree, *J Am Chem Soc* **131**, 17303 (2009).
- [19] L. Qian and E. Winfree, *Science* **332**, 1196 (2011), 10.1126/science.1200520.
- [20] S. M. Chirieleison, P. B. Allen, Z. B. Simpson, A. D. Ellington, and X. Chen, *Nat. Chem.* **5**, 1000 (2013).
- [21] K. Montagne, R. Plasson, Y. Sakai, T. Fujii, and Y. Rondelez, *Mol Syst Biol* **7**, 466 (2011), doi: 10.1038/msb.2010.120.
- [22] J. Kim and E. Winfree, *Mol Syst Biol* **7**, 465 (2011), 10.1038/msb.2010.119.
- [23] T. Fujii and Y. Rondelez, *ACS Nano* **7**, 27 (2013), doi: 10.1021/nn3043572.
- [24] A. Padirac, T. Fujii, and Y. Rondelez, *Proc. Natl. Acad. Sci. USA* (2012), doi: 10.1073/pnas.1212069109.
- [25] A. Padirac, T. Fujii, A. Estévez-Torres, and Y. Rondelez, *J. Am. Chem. Soc* **135**, 14586 (2013), doi: 10.1021/ja403584p.
- [26] a) bounded growth, i.e. there exists $A_{\max} > 0$ such that $r(A_{\max}) = 0$, b) $r(0) = 0$, c) $r'(0) > 0$, and on $(0, A_{\max})$ d) $r(A) > 0$, f) $r'(A) < r'(0)$.
- [27] A. Kolmogoroff, I. Petrowsky, and N. Piscounoff, *Bull. Univ. Moskou, Ser. Internat., Sec. A* **6**, 1 (1937).
- [28] D. G. Aronson and H. F. Weinberger, “Nonlinear diffusion in population genetics, combustion, and nerve pulse propagation,” in *Partial differential equations and related topics* (Springer, Berlin, 1975) pp. 5–49.
- [29] See Supplemental Material at [URL will be inserted by publisher] for the derivation of (2).
- [30] See Supplemental Material at [URL will be inserted by publisher] for additional methods.
- [31] See Supplemental Material at [URL will be inserted by publisher] for Figure S2.
- [32] See Supplemental Material at [URL will be inserted by publisher] video S1 and S2.
- [33] In independent experiments we obtained $D_A = (18 \pm 3) \times 10^3 \mu\text{m}^2/\text{min}$, $D_T = (11.8 \pm 0.8) \times 10^3 \mu\text{m}^2/\text{min}$ and $K = 100 \text{ nM}$ at 44°C .
- [34] W. van Saarloos, *Phys. Rep.* **386**, 29 (2003).
- [35] H. H. Paradies, *J. Phys. Chem* **84**, 599 (1980), doi: 10.1021/j100443a008.
- [36] See Supplemental Material at [URL will be inserted by publisher] for video S3.
- [37] Control measurements of enzymatic activity demonstrated that for both templates the polymerization rates were identical, while nicking rates differed by a factor 3. Considering that polymerization is the rate-limiting step these data demonstrate that the triton drag modifies diffusion while having a negligible influence in the growth kinetics.
- [38] See Supplemental Material at [URL will be inserted by publisher] for video S4.
- [39] D. Scalise and R. Schulman, *Technology* **02**, 55 (2014), doi: 10.1142/S2339547814500071.